Long-time stress relaxation of rubber networks under large uniaxial tension: Effects of strain, cross-link density and filler amount

Haluk Konyali,[a,b] Yusuf Menceloglu[a] and Burak Erman[c]

[a] Sabanci University, Faculty of Engineering and Natural Sciences,
Tuzla 34956 İstanbul, Turkey

[b] Tekno Kaucuk, GOSB, İhsan dede cad. Gebze 41480 Kocaeli, Turkey

[c] Koc University, Department of Chemical and Biological Engineering,
Rumelifeneri Yolu, Sariyer 34450 Istanbul, Turkey

Abstract

Poly-isoprene networks with different degrees of cross-linking and filler amount are studied under uniaxial stress relaxation. Time decay of stress obeys a stretched exponential form with a stretching parameter of 0.4 that is same for all independent variables, i.e., extensions, cross-link density and filler amount. Relaxation time τ increases with increasing strain, and decreases with both cross-link and filler content. Dependence of τ on filler content is less sensitive than on cross-link density. The isochronous Mooney-Rivlin plots show that the phenomenological constant $2C_1$ is time independent, and all time dependence results from that of $2C_2$, which is associated with relaxation of intermolecular interactions at and above the length-scales of network chain dimensions. The relatively low value of the stretching parameter is interpreted in terms of a molecular model where entanglements contribute to relaxation at a wide spectrum of time scales.

Keywords: Entanglements, junction fluctuations, viscoelasticity.

Introduction

According to the molecular interpretation of the elasticity of a random elastomeric network, the force f on a uniaxially stretched system is the sum of two components[1].

$$f = f_{\text{intra}} + f_{\text{inter}} \tag{1}$$

where, f_{intra} is the sum of the elastic contributions of the individual network chains, and f_{inter} is the intermolecular contribution in excess of the intra-molecular component. At equilibrium, the phantom network model of rubber elasticity describes the network in the presence of intra-molecular contributions only. For uniaxial force the reduced force, $[f^*]$, given by this model is

$$[f^*]_{ph} \equiv \frac{f_{\text{intra}}}{\left(\lambda - \lambda^{-2}\right)} = \left(\frac{\xi kT}{V_0}\right) \tag{2}$$

where, ξ is the cycle rank of the network, i.e., the number of chains to be cut to reduce it to a tree, k is the Boltzmann constant, T is the absolute temperature, V_0 is the volume of the network in the reference state, and λ is the extension ratio[1]. This expression is based on the molecular picture where the end-to-end vector of the network chains exhibit a Gaussian distribution.

The Mooney-Rivlin equation, on the other hand, is a phenomenological expression that gives the reduced force as the sum of (i) deformation independent and (ii) dependent components as

$$[f^*] = 2C_1 + 2C_2\lambda^{-1} \tag{3}$$

The Mooney-Rivlin form is particularly attractive because it gives a straight line when $[f^*]$ is plotted as a function of λ^{-1}, where $2C_1$ becomes the intercept and $2C_2$ becomes the slope[1]. If intermolecular contributions vanish in the limit of infinite extension, then the $2C_1$

coefficient may be interpreted as $2C_1 = [f^*]_{ph} = \left(\frac{\xi kT}{V_0}\right)$. If not, then there will be contributions from trapped entanglements. The extent of the contributions from intermolecular effects can be estimated only by well-designed experiments. Some experiments[2] show that the $2C_1$ value leads to the network cycle rank only, and others show that contributions from chain entanglements trapped in the system during cross-linking, i.e., intermolecular effects in the limit of infinite extension are present[3]. The experiments of Rennar and Oppermann [4] showed the conditions under which trapped entanglements are important in a conclusive manner. Whether the $2C_1$ value leads to the phantom network value or not is not of interest in the present study. Here, we study the relaxation behavior of the $2C_1$ and $2C_2$ values under a sudden uniaxial force until they reach constant values independent of time.

The $2C_2$ term is unequivocally accepted as representative of intermolecular contributions to the deformation dependent part of the reduced force. It results from intermolecular contributions that perturb the chain conformations when an external deformation is applied. It results from rearrangements at larger length scales, such as length-scales of the end-to-end vector and larger, and therefore its dynamics is expected to be easily separated from that of $2C_1$ that operates at length scales of entanglements. The relaxation experiments of Noordermeer and Ferry on polybutadiene networks showed that the relaxations of $2C_1$ and $2C_2$ are indeed separated over time[5]. Since ϕ network chains meet at a ϕ-functional junction, the intermolecular contributions to elasticity may equally be studied in terms of the perturbations of the junction positions from those of the phantom network model. Graessley, Edwards et. al, adopted the former[6, 7], and Flory and collaborators adopted the latter picture[8-10]. That the two representations reduce to the same result have been shown by Vilgis and Erman some years ago[11].

In the present experimental work, we study the effects of cross-link density and filler amount on the elasticity of random amorphous networks that are slightly put out of equilibrium by imposing a sudden uniaxial extension, where the force required to hold the sample at that constant elongation is measured. The aim of the study is to observe and quantify the deviations from the equilibrium state, using the phenomenological Mooney-Rivlin equation

and the associated molecular interpretation. The independent variables are the extension ratio, cross-link density, and amount of filler. The dependent variable is the force, as a function of time, required to keep the samples at fixed length. We consider 'long-time' stress relaxation where fast local motions relating to the sub-chains of a given network chain are already equilibrated, and only long-time rearrangements of the network end-to-end distances are active. Below, we give a more specific definition of 'long-time' relaxation.

At equilibrium, a network junction exhibits large-scale fluctuations about its mean position. This is because the pendent chains to the junction exhibit large-scale diffusive motions about their equilibrium configurations. In a tetra-functional phantom network, the mean squared fluctuations $\left\langle (\Delta R)^2 \right\rangle$ of a junction is related to the mean-squared end-to-end distance $\left\langle r^2 \right\rangle_0$ of a network chain by[12] $\left\langle (\Delta R)^2 \right\rangle = \frac{3}{8}\left\langle r^2 \right\rangle_0$. For a network with $[f^*] = 0.1\,Nmm^{-2}$, the radius of the fluctuation domain for a polyisoprene chain is about there are about 50 cross-links that share this domain. At sufficiently long time scales corresponding to the equilibrium state, the radius of the spherical domain in which a junction fluctuates equates to about 50 Å. At equilibrium, the ϕ pendent network chains, for a ϕ functional network, move from one conformation to the other and the junction explores all possible points in its spherical fluctuation domain. However, immediately following a sudden macroscopic extension, the chains are in states close to frozen and the junction does not have a chance to explore all points in this domain. As the network is allowed to relax, the junction explores larger and larger regions of the constraint domain. The process may be followed easily through the time dependence of the $2C_1$ and $2C_2$ parameters where the former reflects the dynamics operating at length scales of $\left[\left(\frac{M_e}{M_c}\right)\left\langle r^2 \right\rangle_0\right]^{1/2}$ while the latter reflects the dynamics at length scales of $\left\langle r^2 \right\rangle_0$ or larger. Here, M_e is the entanglement molecular weight, M_c is the molecular weight of a network chain, and $\left\langle r^2 \right\rangle_0$ is its unperturbed mean-squared end-to-end distance. The relative behaviors of $2C_1$ and $2C_2$ depends on the distance of the system from its glass transition temperature. In earlier work, on stress relaxation of poly-butadiene networks, … and Ferry observed that during the initial stages of relaxation the $2C_1$ values decreased while the $2C_2$ values were constant. During later stages of relaxation, $2C_1$ values remained constant

while the $2C_2$ values relaxed until equilibrium. Our present experimental results on poly-isoprene networks at room temperature show that the $2C_1$ term is time independent, irrespective of the degree of cross-linking and filler content, and only the $2C_2$ varies with time.

Experimental:

Materials used

The raw materials used in this recipe were Natural rubber (polyisoprene) , Carbon black, Zinc Oxide, Stearic Acid, CBS (N-cyclohexyl-2-benzothiazole sulphenamide) and Sulfur. All the raw materials were used as received. The natural rubber grade was Ribbed Smoked Sheet, RSS1, with a Mooney viscosity of 85 Mooney Units, MU, at 100°C (1+4), supplied from Eversharp Rubber Industries, Jalan, Singkang, Jementah, Johor. The carbon black grade was HAF N 330 from Tüpraş (www.tupras.com.tr). The DBP (dibutylphthalate) absorption of the carbon black was 116,4 ml/100g, the iodine adsorption was 45,6 mg/g, the ash content was 0,2 and the humidity was 0,11 %. Zinc oxide, 99,7 % purity with a 550 g/l bulk density was supplied from Metal Oksit (www.metaloksit.com). Stearic acid with an acid value 208,8 mg KOH/g, fatty acid composition 55,2 % C16, 44,2% C18 was supplied from Natoleo (www.natoleo.co.kr). CBS was supplied from MLPC. Its melting point was 97°C, ash content was 0,3% and specific gravity was 1,27. Sulfur was supplied from MLPC (www.mlpc-intl.com). Its melting point was 115 °C and specific gravity was 2,04.

Compounding

Compounds were prepared by using a lab scale 1,5 liter Werner & Pfleiderer internal mixer. This internal mixer has standard tangential rotor geometry. The homogenizations were made on the two roll open mills. The master batch was prepared with a fill factor of 0,85 in the internal mixer. Rubber was fed into the chamber, masticated for 2 minutes and then Zinc Oxide and Stearic acid were added. The compound was dumped at around 135 °C. It homogenized on the two roll mill for 5 minutes. In the second stage, accelerator, sulfur and additional carbon black were added on the two roll mill for different compounds.

Vulcanization

Vulcanization was carried out in a compression molding with 160 t clamping force. All test sheets were vulcanized at 150°C/ 35min. The test sheet dimensions were 210x300x2 mm^3.

Relaxation tests

All 2 mm thick dumbbell shaped test sheets were cut out from these vulcanized sheets with the help of a Zwick sample cutter. The dumbbell shaped test sheet was in accordance with DIN 53 504, S1. The relaxation tests were carried out in an universal tensile machine (UTM). The brand name was Zwick Roell Z2,5. Its load cell was 2,5 kN. This machine had also an extensometer that acquired data at every 10 microns with an accuracy of 1%. The equipment used testXpert V10.1 version software. Dumbbell shaped test sheets were tested at UTM with a pre-load of 0,2 N that prevented the initial curvature of the free samples. Test sheets were stretched to different extension ratios at a speed of 800 mm/min, and relaxed for 800 sec. for every sample. Data was taken at every 0,02 s. during the test. In order to simplify presentation, we use the notation in Table 1 for sample designation.

Table I. Sample Notation

	Amount of filler, phr				
Amount of cross-linker phr		**0**	**5**	**10**	**15**
	0.75	S_{11}	S_{12}	S_{13}	S_{14}
	1.0	S_{21}	S_{22}	S_{23}	S_{24}
	1.25	S_{31}	S_{32}	S_{33}	S_{34}

Results and Discussion

In Figs. 1.a-d we present isochronous Mooney-Rivlin plots for networks with different cross-link densities and different filler contents. Fig. 1.a shows the results for the network S_{11} with no filler and low degree of cross-linking. The sulfur content used in cross-linking this sample corresponds to network chains of $M_c = 1.4x10^4$ $gmol^{-1}$ (conversion rate for the unfilled samples is: 1 phr = $1.05x10^4$ $gmol^{-1}$)[1] The shortest time of observation is one second. The longest time of 800 seconds recorded in the experiments did not correspond to full equilibrium, but sufficiently close to it for all of the samples. The best fitting straight line is drawn through each set of isochronous data. As time progresses, the $2C_1$ intercept remains approximately constant while the slope $2C_2$ decreases. If the samples were stretched much

faster than the network chains could rearrange or at temperatures close to T_g, then the dynamic entanglements operating along the network chains would act as additional cross-links, and this would lead to higher values of $2C_1$ that would then decrease with relaxation. Indeed, earlier experiments of Ferry and collaborators on poly-butadiene networks show this effect. These short time scales are the ones during which chain-chain entanglements play dominant role in relaxation. The time scales in which the $2C_1$ values remain fixed and only $2C_2$ values change may be accepted as the long-time relaxation regime during which relaxation takes place through conformational rearrangements of the network chain end-to-end vector distributions towards their equilibrium values.

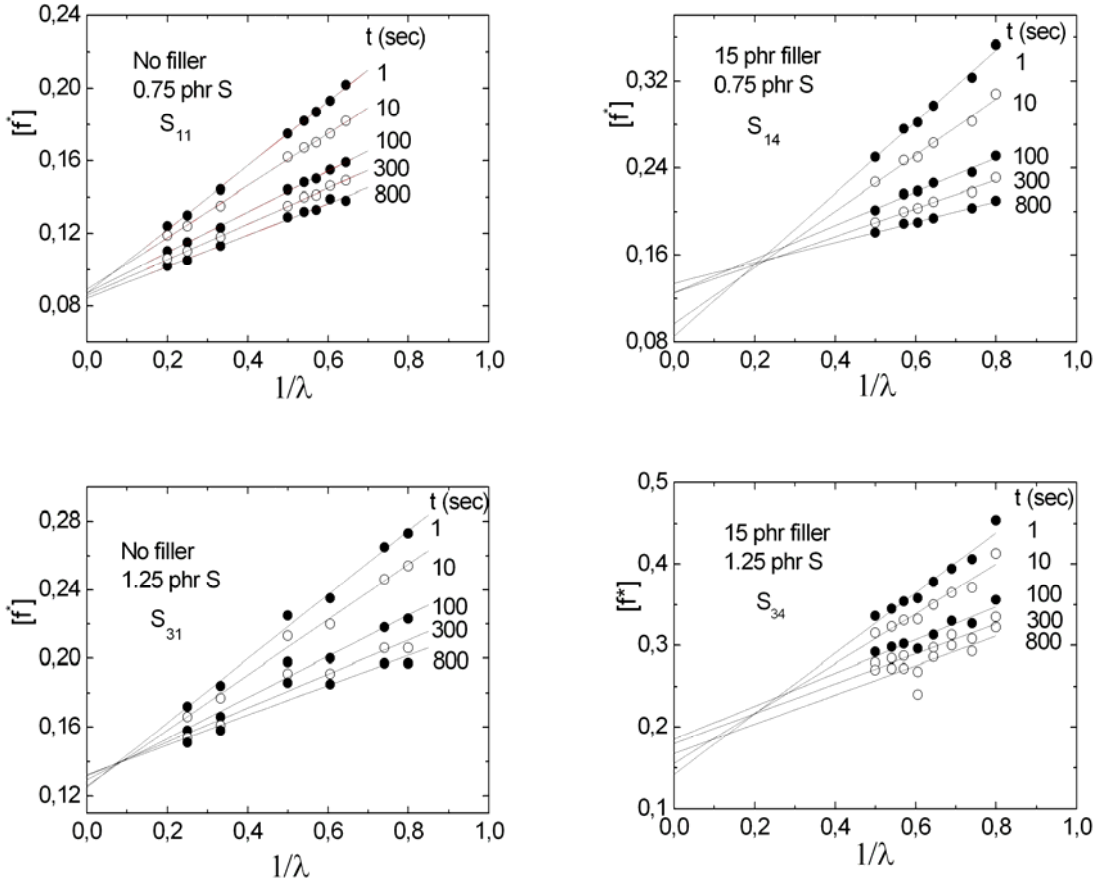

Fig. 1.a-d Isochronous Mooney-Rivlin plots of Samples S_{11}, S_{14}, S_{31} and S_{34}.

In Fig. 1.b, isochronous Mooney-Rivlin plots are presented for the sample S_{14} with the same degree of cross-linking and highest amount of filler. In Fig. 1.c similar curves are given for the samples S_{31} and S_{34} with highest degree of cross-linking. In all cases the points exhibit the

straight line behavior in which the $2C_2$ values decrease in time and $2C_1$ values are approximately constant. Only in the case of highest filler samples, S_{14} and S_{34}, the $2C_1$ values intersect in around λ^{-1}=0.2, instead of the expected zero intercept. This is possibly due to inaccuracies of short time measurements that become increasingly difficult as the degree of cross-linking increases. It is interesting that the addition of filler affects the $2C_1$ values much less significantly than the $2C_2$ values. For the lowest degree of cross-linking, the $2C_1$ intercepts are 0.08 and 0.08-0.13 for S_{11} and S_{14}, respectively. The corresponding $2C_2$ values are 0.18 and 0.33. For the highest degree of cross-linking, the $2C_1$ intercepts are 0.13 and 0.14-0.18, respectively, whereas the he corresponding $2C_2$ values are 0.18 and 0.36. In summary, filler amount has significant effect of the $2C_2$ values, and much lesser effect on $2C_1$.

In Fig. 2.a the dependence of the $2C_1$ values on time are plotted for the highest cross-link density sample for different values of filler amount. Similarly, in Fig. 2.b, the dependence of $2C_2$ on time is presented. The curves are given for the lowest cross-link values, but the same trend is present for higher degrees of cross-linking. Fig. 2.a clearly shows that within the time scales of the present experiments, except the highest cross-link highest filler sample S_{34}, the $2C_1$ values have already reached constant values. The $2C_2$ values, on the other hand describe the slow relaxation behavior fully. The time decay of $2C_1$ for S34 indicates that relaxations in the sub-M_e scale are still active.

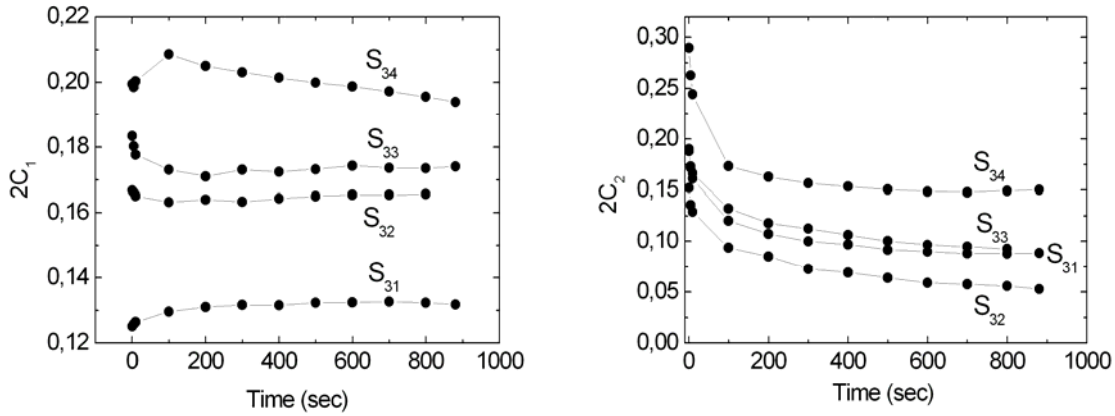

Fig. 2. a and b. The time dependence of $2C_1$ and $2C_2$

Our results show that the dependence of stress, σ (defined as the force per unit undeformed cross-sectional area) on time during slow relaxation exhibits a definite stretched exponential form

$$\sigma(t) = \sigma_\infty + (\sigma_0 - \sigma_\infty) e^{-\left(\frac{t}{\tau}\right)^{0.4}} \qquad (4)$$

where, σ_∞ is the equilibrium stress and σ_0 is the stress at zero time. Results for the unfilled sample S_{11} and for the highest filler sample S_{14} are presented in Figs. 3.a and b, respectively.

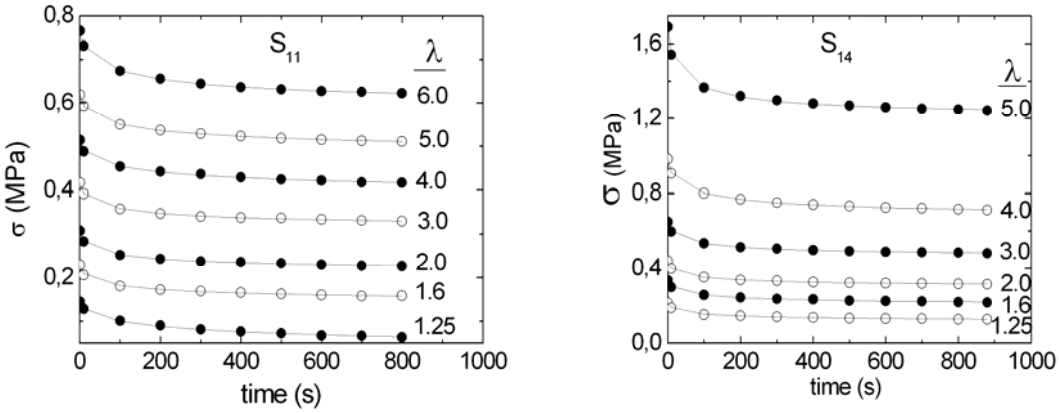

Figure 3. Dependence of stress on time.

The lines are obtained from Eq. 4, the points are experimental. As is evident from the figures, the value of 0.4 for the exponent leads to perfect agreement between experiment and Eq. 4 for all times. In the interest of brevity, we present results for the samples S_{11} and S_{14}, only. Results for all the other samples are in perfect agreement with the exponent 0.4.

The parameters of Eq. 4 are determined as follows: First an initial value m for the exponent is chosen. For each extension ratio, the value τ of the relaxation time is assumed, and the variable $x = e^{-\left(\frac{t}{\tau}\right)^{\beta}}$ is calculated for each time. With the use of x defined in this manner, Eq. 4 takes the following linear form $\sigma(t) = A + Bx$, where $A = \sigma_\infty$ and $B = (\sigma_0 - \sigma_\infty)$. The value of τ that led to the best agreement between experimental data and the straight line determined A and B. Calculations were repeated for different exponent values. Best linear fits

were obtained for the exponent β = 0.4. In the Appendix, we tabulate the values of σ_∞, $(\sigma_0 - \sigma_\infty)$, and τ for different extension ratios for the lowest and highest filler samples.

The relaxation times obtained by fitting experimental data to Eq. 4 exhibit strong deformation dependence. The general trend is that increasing strain increases the relaxation times. In Figure 4, the dependence of relaxation times for three different cross-link densities of unfilled samples is presented. In Figure 5, relaxation times are plotted.

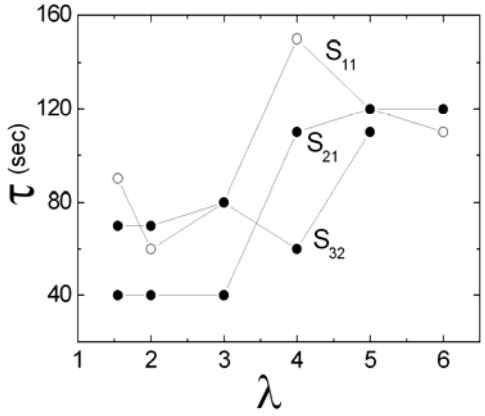

Figure 4. Relaxation time as a function of extension ratio for different cross-link densities.

In Figure 5, the effects of filler on the relaxation times for different extension ratios are shown.

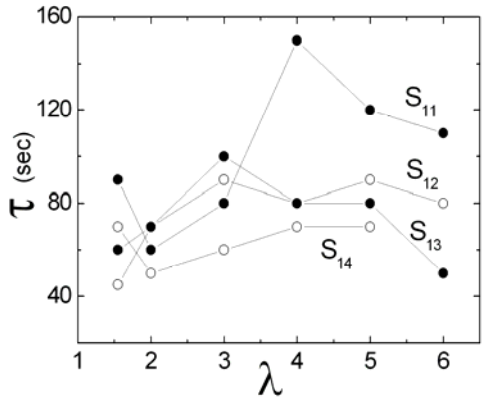

Figure 5. Effect of filler on relaxation times for the lowest cross-link density sample.

In Figure 6, a summary is given where the relaxation times are averaged over all cross-link values (the unfilled circles) for the unfilled sample, and over all filler amounts (filled circles) of the lowest cross-link density, presented as a function of extension ratios. It is to be noted

that values for $\lambda = 1.25$ are not shown in figures 4-6 because this low degree of deformation lead to large scatter in relaxation time values, probably due to large source of error in force and deformation measurements, and possibly due to the existence of a different regime of slow relaxation at low deformation. The accuracy of our measurements at small deformations is not sufficient to give a definitive explanation for this behavior, and more detailed experiments at higher accuracy are required. The increase of relaxation times with increasing deformation observed in Figs. 4-6 indicates that relaxation slows down as the anisotropy of the system increases under increasing uniaxial extension.

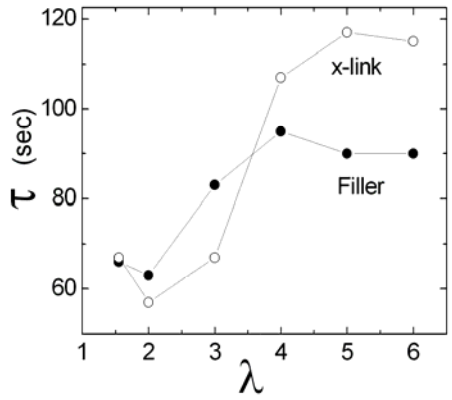

Figure 6. Effects of cross-link and filler amounts on relaxation times at different extension ratios.

In Figure 7, the effects of filler amount and cross-linker amount on the relaxation times are shown. The same amount of decrease from 120 s to 60 s in relaxation time is observed when either the filler amount is increased from 0 and 15 phr or the cross-linker is increased from 0.75 and 1.25 phr. Thus, changes in relaxation time are much more sensitive to changes in cross-link density than to filler amount.

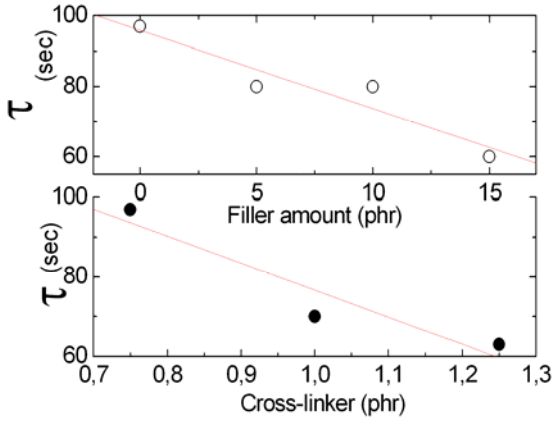

Figure 7. Effects of cross-link and filler amounts on relaxation times averaged over extension ratios.

The data presented in Fig. 7 indicates that there is a correspondence between the effects of cross-linker and filler amounts on relaxation times, somewhat similar to the time-temperature correspondence in viscoelasticity.[13]

The radii of the fillers used in the samples were between 500-6000 Å, whereas the entanglement domains have radii of 50 Å. Thus, the length-scales of filler and constraint domains responsible for the relaxation of $2C_2$ are widely separated. On the other hand, changing the cross-link density directly affects the mean-squared dimensions of the fluctuation domain given by the expression[12]

$$\left\langle (\Delta R)^2 \right\rangle = \frac{3}{8}\left\langle r^2 \right\rangle_0 = \frac{3}{8} C_\infty n l^2 \qquad (5)$$

Where, n is the number of repeat units of a network chain, C_∞ is the characteristic ratio of the chain, and l is the length of a repeat unit. The proportionality of the constraint domain size to network chain dimensions indicated by Eq. 5 implies that relaxation times are expected to be more sensitive to changes in cross-link density than to changes in filler amount. This is indeed indicated by the present experiments shown in Fig. 7.

Finally, we would like to point out that the stretched exponent behavior of relaxation, which is phenomenologically known as Williams-Watts-Kohlrauch form, may be taken as an indication of serial cooperativity where different pathways of relaxation exist in which one

relaxation step depends on the occurrence of another. Stated in another way, relaxation goes through hierarchically constrained steps: Sudden stretching of the network causes an affine-like deformation of chains. Chains deformed in this manner do not relax all at once. A group of chains relax first, this induces the relaxation of others, through network connectivity. Thus, according to this interpretation, relaxation propagates from one junction to its topological neighbors in a serial fashion. We would like to indicate that this interpretation, although plausible, is one of several other possible relaxation pathways. This type of hierarchical relaxation was introduced by Palmer et. al., [14] and since then has been adopted for the relaxation in a diverse field of materials.

In order to understand the molecular basis of long-time relaxation, we consider the relaxation components of a junction in more detail: A junction is embedded into the ϕ-functional network by means of ϕ chains. The size of the fluctuation domain of the junction is determined by the fluctuations of the ϕ pendent chains and the rest of the network to which these ϕ chains are attached. As briefly stated above, the system deforms close to affine when a sudden stretch is applied to the network. The chains and the junctions are close to frozen at the initial state due to the hindrance of entanglements. As the system relaxes, the junction explores different points in its fluctuation domain. We term this 'the relaxation of the junction'. The excursions of the junction are obviously a result of the fluctuations of the pendent chains. The pendent chains perform their fluctuations under the presence of intermolecular effects, i.e., entanglements. The entanglements on chains can be transferred to the junction most pronouncedly if the junction is part of a cycle as shown in Fig. 8. In fact, in a perfect network, there are several cycles of different length that affect the fluctuations of a junction. In Fig. 8, a cycle of length 6 is shown. The circle shows the fluctuation domain of junction i. The center of this domain is indicated by O. The vector ΔR_i indicates the

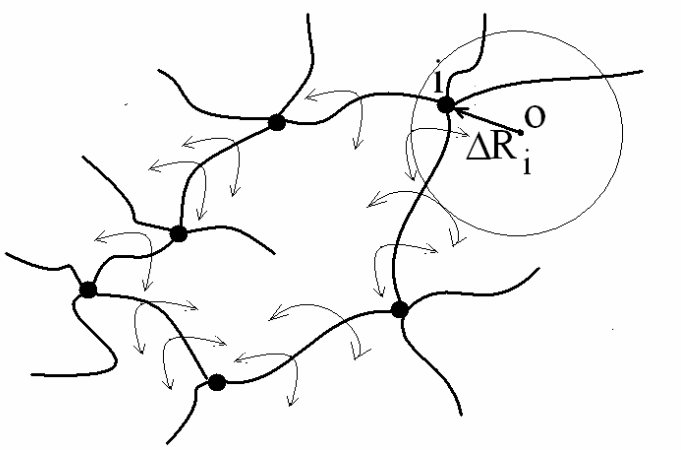

Figure 8. Fluctuations of the junction i under the effects of entanglements.

instantaneous fluctuation of the junction from its center. The distribution of ΔR_i will be time dependent in a relaxing network. This time dependent distribution will relax to the time independent distribution as equilibrium is approached. Cycles of different length are expected to contribute differently to the relaxation of the junction. Longer cycles are subject to a larger number of chain entanglements and hence their contribution to relaxation will be spread over longer time scales. Shorter cycles with only a few entanglements will be the fastest relaxation contributors. If the relaxation time associated with a cyclic path is τ_i and the contribution of this path to relaxation is $g(\tau_i)$, then the stretched exponential form, may be written as

$$e^{-\left(\frac{t}{\tau}\right)^{\beta}} = \sum_i g(\tau_i) e^{-\left(\frac{t}{\tau_i}\right)} \tag{6}$$

where, the left hand side is determined by the experimentally determined τ and β. Once these parameters are known, the distribution function $g(\tau_i)$ may be calculated by[15]

$$g(\tau_i) = \frac{1}{\pi\tau} \sum_{k=1}^{\infty} \frac{(-1)^k}{k!} \sin(\pi\beta k)\Gamma(\beta k + 1)\left(\frac{\tau_i}{\tau}\right)^{\beta k} \tag{7}$$

Here, $\Gamma(\ )$ is the gamma function. For $\beta = 0.4$ and $\tau = 1$, the distribution function is calculated from Eq. 7 and is shown in Fig. 9. The peak contribution is equal to 0175 and is around $\tau_i = 2$. However, the relaxation times are spread over a large range. Even at a relaxation time of 20, the amplitude is 0.06 which is significant. According to the molecular

model described above, such large relaxation times are those that result from entanglements along long cyclic paths.

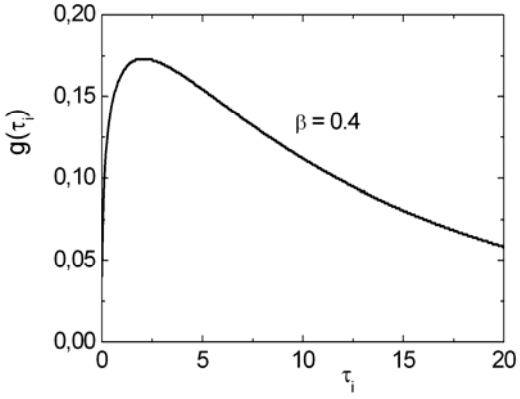

Figure 9. The spectrum of relaxation times for the exponent b = 0.4.

Appendix: Values of σ_∞, $(\sigma_0 - \sigma_\infty)$, and τ for different extension ratios for the lowest and highest filler samples.

Sample S_{11}

λ	σ_∞ (MPa)	$(\sigma_0 - \sigma_\infty)$ (MPa)	τ (s)
1.25	0.0375	0.1196	300
1.6	0.1502	0.0903	90
2	0.2221	0.1028	60
3	0.3215	0.1114	80
4	0.3991	0.1294	150
5	0.4941	0.1444	120
6	0.6014	0.1914	110

Sample S_{21}

λ	σ_∞ (MPa)	$(\sigma_0 - \sigma_\infty)$ (MPa)	τ (s)
1.25	0.1023	0.0571	40
1.6	0.1815	0.0752	70
2	0.2539	0.0911	70
3	0.3612	0.1046	80

4	0.4673	0.1112	60
5	0.5882	0.1470	60

Sample S_{31}

λ	σ_∞ (MPa)	$(\sigma_0 - \sigma_\infty)$ (MPa)	τ (s)
1.25	0.1152	0.0618	80
1.6	0.1869	0.0727	40
2	0.3248	0.0884	40
3	0.4545	0.1007	40
4	0.5830	0.1091	110
5	0.5818	0.1095	120
6	0.8200	0.2264	120

Sample S_{12}

λ	σ_∞ (MPa)	$(\sigma_0 - \sigma_\infty)$ (MPa)	τ (s)
1.25	0.0965	0.0761	40
1.6	0.1674	0.1027	45
2	0.2367	0.1228	70
3	0.3382	0.1352	90
4	0.4259	0.1492	80
5	0.5371	0.2010	90
6	0.8014	0.3236	80

Sample S_{13}

λ	σ_∞ (MPa)	$(\sigma_0 - \sigma_\infty)$ (MPa)	τ (s)
1.25	0.0954	0.1012	50
1.6	0.1694	0.1155	60
2	0.2511	0.1375	70
3	0.3603	0.1595	100
4	0.4973	0.2136	80
5	0.6919	0.3348	80
6	1.0525	0.4997	50

Sample S_{14}

λ	σ_∞ (MPa)	$(\sigma_0 - \sigma_\infty)$ (MPa)	τ (s)
1.25	0.1232	0.1103	60
1.6	0.2114	0.1466	70
2	0.3106	0.1550	50
3	0.4723	0.2112	60
4	0.6935	0.3426	70
5	1.2304	0.5733	40

References

1. Mark, J.E. and B. Erman, *Rubberlike Elasticity: A Molecular Primer.* 2007: Cambridge University Press.
2. Erman, B., W. Wagner, and P.J. Flory, Macromolecules, 1980. **13**: p. 1554.
3. Langley, N.R. and K.E. Polmanteer, J. Polym. Sci., Polym. Phys. Ed., 1974. **12**: p. 1023.
4. Rennar, N. and W. Oppermann, *Model PDMS, II, C&PS.* Coll. Polym. Sci., 1992. **270**: p. 527.
5. Noordermeer, J.W.M. and J.D. Ferry, *Nonlinear relaxation of stress and birefringence in simple extension of 1,2-polybutadiene.* J. Polym Sci. Polym. Phys.Ed., 1976. **14**: p. 509-520.
6. Edwards, S.F. and T.A. Vilgis, *Elasticity Rev., Rep. Prog. Phys.* Rep. Prog. Phys., 1988. **51**: p. 243.
7. Graessley, W.W. and L.M. Dossin, *Doi-Edwards theory ext to networks.* Macromolecules, 1979. **12**: p. 123.
8. Erman, B. and P.J. Flory, *Experimental Results. p 607.* Macromolecules, 1983. **16**: p. 1607.
9. Erman, B. and P.J. Flory, *Relationship between Stress, Strain, and Molecular Constitution of Polymer Networks. Comparison of Theory with Experiment.* Macromolecules, 1982. **15**: p. 806.
10. Flory, P.J. and B. Erman, *Theory of Elasticity.* Macromolecules, 1982. **15**: p. 800.
11. Vilgis, T.A. and B. Erman, *Constrained-J. vs. Slip Link Models.* Macromolecules, 1993. **26**: p. 6657.
12. Erman, B. and J.E. Mark, *Structures and Properties of Rubberlike Networks*. 1997, New York: Oxford University Press.
13. Ferry, J.D., *Viscoelastic Properties of Polymers*. 3rd ed. 1980, New York: Wiley.
14. Palmer, R.G., et al., *Models of hierarchically constrained dynamics for glassy relaxation.* Phys. Rev. Lett., 1984. **53**: p. 958-961.
15. Lindsey, C.P. and G.D. Patterson, *Detailed comparison of the Williams-Watts and Cole-Davidson functions.* Journal of Chemical Physics, 1980. **73**: p. 3348-3357.